10528 *Macromolecules* **2010**, *43*, 10528–10535
DOI: 10.1021/ma1015209

Macromolecules
ARTICLE

Ordering in Mixtures of a Triblock Copolymer with a Room Temperature Ionic Liquid

Daniel F. Miranda, Thomas P. Russell,* and James J. Watkins*

Polymer Science and Engineering Department, University of Massachusetts, Amherst, Massachusetts 01003, United States

Received July 7, 2010; Revised Manuscript Received October 20, 2010

ABSTRACT: Well-ordered block copolymer (BCP) morphologies are obtained by blending PEO−PPO−PEO triblock copolymer surfactants with the room temperature ionic liquid (IL) 1-butyl-3-methylimidazolium hexafluorophosphate. The selective association of the IL with the PEO blocks increases the segregation strength by raising the effective interaction parameter between the PEO and PPO blocks. Therefore, the copolymer/IL blends form well-ordered microdomains in the melt, whereas the neat copolymers are phase mixed. The IL is shown to interact with the PEO chains of the copolymers by a depression in the melting point of the PEO crystals with increasing IL concentration. Wide-angle X-ray diffraction and polarized optical microscopy also show a disruption of PEO crystallization in the copolymer/blends. Infrared spectroscopy indicates a favorable enthalpic interaction between the PEO blocks and the IL, which does not exist between PPO and the IL. Small-angle X-ray scattering confirms the enhanced ordering of the copolymers upon addition of the IL, the formation of well-ordered microdomains, and a change in the characteristic spacing with increasing IL concentration.

Introduction

Microphase-separated block copolymers (BCPs) have attracted considerable interest due to their ability to self-assemble into ordered periodic structures.[1,2] To increase the degree of microphase separation, a phase selective additive can be incorporated into the copolymer that selectively partitions into a single copolymer microdomain. This enhances the nonfavorable interactions between the blocks of the copolymer, increasing the segregation strength. Recent work has shown that the addition of a selectively interacting homopolymer can induce microphase separation of a low molecular weight $PEO_nPPO_mPEO_n$ triblock copolymer.[3,4] Salt complexation has also been shown to have a significant effect on BCP morphology, in the bulk[5,6] and in thin films.[7−9] The salts selectively interact with one block of the copolymer, increasing the effective interaction parameter, χ_{eff}. Small molecule phase selective diluents and solvents have also been used to alter the morphology of a BCP and have been extensively studied.[10−18]

Room temperature ILs are typically composed of large molecular cations and anions. The asymmetry and conformational flexibility of these ions result in small lattice energies that depress the melting point.[19] ILs have been termed "designer solvents," as the properties of an IL vary considerably between different cation and anion pairs.[20] With over 1 million IL combinations possible, it is conceivable that an IL can be engineered specifically for a particular application or reaction.[21] Many reviews regarding the properties and applications of ionic liquids have been published, several of which are cited here.[21−23]

In addition to low melting temperatures and negligible volatility, ILs have several other interesting properties, including high thermal stability, high ionic conductivity, and large electrochemical windows.[22,24−27] These properties are desirable for electrolytes,[28] and as such, ILs have attracted considerable interest as potential electrolytes for dye-sensitized solar cells,[29−32] fuel cells,[33−35] and lithium ion batteries.[36−39] There has also been considerable effort devoted to the gelation of ILs for applications as solid polymer electrolytes[23,40,41] and stimuli responsive gels.[23]

ILs have also been employed to induce the self-assembly of block copolymer amphiphiles and surfactants. IL selectivity for the polar hydrophilic block has been demonstrated to induce self-assembly into ordered BCP microphases[42−44] and into core−corona micelles for solutions of BCPs in ILs.[45−47] Triblock copolymers with PS end blocks and IL coordinating midblocks form gels with physical PS cross-links when swollen with an IL.[41,48] Pluronic copolymer surfactants have also been demonstrated to self-assemble into ordered BCP microphases[49,50] and into micelles.[51−54] Self-assembly of other nonionic surfactants in ILs has also been extensively studied.[55−60]

In this work, copolymers from the Pluronic series of nonionic surfactants are blended with the room temperature IL 1-butyl-3-methylimidazolium hexafluorophosphate ([BMI][PF_6]). Pluronic surfactants, low cost, low molecular weight PEO_n-*b*-PPO_m-*b*-PEO_n triblock copolymers, having a range of molecular weights and PEO fractions were used. Previous work has established the selectivity of [BMI][PF_6] for the PEO blocks of several copolymers.[41,42,49] In the present work, this selectivity drives microphase separation in several Pluronic copolymers of varying molecular weight and PEO weight fractions, as demonstrated by small-angle X-ray scattering. Differential scanning calorimetry and infrared spectroscopy were used to characterize the nature and strength of the interactions. Polarized optical microscopy and wide-angle X-ray scattering were used to characterize the effect of the IL on PEO crystallinity. These results provide clear evidence for the formation ordered ion gels.

Experimental Section

Materials. The Pluronic copolymers used in this work were provided by BASF. Three different copolymers from the Pluronic

*Corresponding authors. E-mail: russell@mail.pse.umass.edu (T.P.R.); watkins@polysci.umass.edu (J.J.W.).

 Published on Web 11/22/2010

Table 1. Polymer Characteristics

polymer	total M_n	wt % PEO	PDI
F108	14600	80	1.21
F127	12600	70	1.19
F77	6600	70	1.09
PEO	4600	100	1.07
PPO	3500	0	1.14

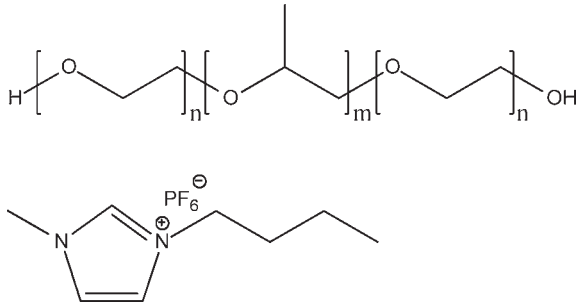

Figure 1. Chemical structure of a typical Pluronic and of [BMI][PF_6].

series were used: F127, F108, and F77. These copolymers are of varying molecular weight and PEO weight fraction. The characteristics of the polymers are summarized in Table 1. The PDI of the Pluronic surfactants used in the study range between 1.07 and 1.21. PEO homopolymer and PPO homopolymer were purchased from Sigma-Aldrich. The molecular weight of the homopolymer was chosen to closely match the block lengths of the corresponding PEO or PPO segments in F127. The Pluronic copolymers and neat PEO are white crystalline solids, and PPO is a colorless viscous liquid. The polymers were dried under vacuum at 70 °C for 24 h prior to use, but were otherwise used as received.

The IL 1-butyl-3-methylimidazolium hexafluorophosphate was purchased from Sigma-Aldrich and used as received. The IL has a melting point of 10 °C and is transparent with a faint yellow color. Sigma-Aldrich specifies less than 200 ppm of moisture and less than 10 mg/kg of halogen impurities. The IL was stored in a nitrogen-purged glovebox, as the IL is hygroscopic.

Blend Preparation. Polymer/IL blends were prepared by mixing the polymer with varying concentrations of IL in a common solvent. For each blend, the appropriate amounts of each component and a stir bar were placed in a vial while in the glovebox and capped with a septum. Outside the glovebox the cosolvent, anhydrous grade *N*,*N*-dimethylformamide (Sigma-Aldrich), was added through the septum, forming 3−4 wt % polymer solutions. The solutions were stirred at ≈40 °C for 3 h. Most of the cosolvent was then evaporated by purging the vial with nitrogen over a period of 24 h. The temperature was increased to 70−80 °C to speed the evaporation. The blends were then dried under vacuum at 70−80 °C for 24 h to remove any remaining cosolvent and residual moisture. The polymer/IL blends were stored in a nitrogen-purged glovebox immediately after drying.

Differential Scanning Calorimetry. 5−15 mg of each blend was added to hermetically sealed aluminum hermetic sample pans for differential scanning calorimetry (DSC). The pans were filled and crimped while in the nitrogen-purged glovebox to seal the pans. The hermetic seal was sufficient to prevent moisture absorption by samples within the DSC pans once the pans are removed from the glovebox.

DSC thermograms were obtained with a model Q200 DSC from TA Instruments, equipped with a liquid nitrogen cooling system (LNCS). Each sample was heated to 80 °C, cooled to −20 °C, and then reheated to 80 °C. The cooling and second heating scans were run at a 5 °C/min ramp rate. Thermograms are reported only from the second heating scan. For blends with high IL concentration (50 wt % and higher in F127 and F108 and 40 wt % and higher in F77), in order to ensure sufficient time for crystallization, it was necessary to hold to blends isothermally at 0 °C for 1 h upon cooling from the first heating step. Melting points are taken as the temperature at which the last trace of crystallinity disappears, i.e., the high temperature end of the endothermic melting peak. The heat flow output from the calorimeter was normalized by the mass of PEO present in the blend. The melting enthalpies were measured by determining the area of the endothermic melting peaks by integration using the Universal Analysis software from TA Instruments. The crystalline fraction can then be calculated by taking the ratio of the melting enthalpy for a particular blend to the heat of fusion for an infinite, perfect PEO crystal (188.9 J/g).[61]

Optical Microscopy. Films for optical microscopy were prepared by drop-casting 5 wt % polymer/IL blend solutions in THF onto glass coverslips. The solvent was removed by drying under vacuum for ∼24 h. The films were then melted on a hot plate, and a second coverslip was added on top of the film. The films were heated for an additional 30 min and then allowed to cool. Films were observed with polarized light on an Olympus BX60 optical microscope. Optical micrographs were obtained 10 days after the addition of the second coverslip and were stored in the glovebox under nitrogen during this time.

Infrared Spectroscopy. Infrared spectra were obtained with a Bruker Tensor 27, equipped with a diamond ATR-IR accessory and an MCT detector. Spectra were obtained from 4000 to 600 cm^{-1} and were averaged over 32 scans with a 4 cm^{-1} resolution. For the neat [BMI][PF_6], a small droplet of the IL was placed directly onto the ATR crystal. For the solid blends and neat polymers, a small amount of each sample was placed onto the crystal and formed into a film using a small press attached to the ATR-IR accessory.

X-ray Scattering. Sample holders for small- and wide-angle X-ray scattering were made from 1.0 mm thick washers with a Kapton film window. Polymer/IL blends were added to the sample holders while in the glovebox. Air gaps were removed by heating the samples to 70−80 °C under vacuum for 24 h. A second Kapton window was adhered to the washer after the heating step to prevent leakage from the sample holder.

Small-angle X-ray scattering (SAXS) experiments were performed in-house using a Molecular Metrology instrument equipped with a 30 W microsource (Bede) with a 30×30 μm^2 spot size matched to a Maxflux optical system (Osmic) producing a low-divergence monochromatic Cu Kα beam (wavelength $\lambda = 0.1542$ nm). The SAXS intensity was collected by a two-dimensional gas-filled wire detector (also from Molecular Metrology) at a distance of about 1500 mm from the sample. The instrument was calibrated for SAXS using the well-known reflection from silver behenate. A homemade heater was used to run the scattering experiments at 70−80 °C to ensure that all samples are in the melt. The 2-D patterns were integrated azimuthally to give a one-dimensional representation of the scattering, with integrated intensity plotted against the scattering vector.

Wide-angle X-ray scattering (WAXS) experiments were performed using the same setup, but with an image plate positioned in the sample chamber at a distance of 139 mm from the sample. The image plate has a hole in its center allowing the direct X-ray beam to pass through. The instrument was calibrated for WAXS using a tricosane standard. The homemade heater was similarly used to obtain WAXS profiles at 70−80 °C as well as for room temperature WAXS profiles.

Results and Discussion

IL/Polymer Interactions. Differential scanning calorimetry provides a means to assess the miscibility of the IL in neat PEO and Pluronic copolymers. By measuring the melting point depression and reduction in crystallinity, the strength of the interaction between the polymers and IL can be

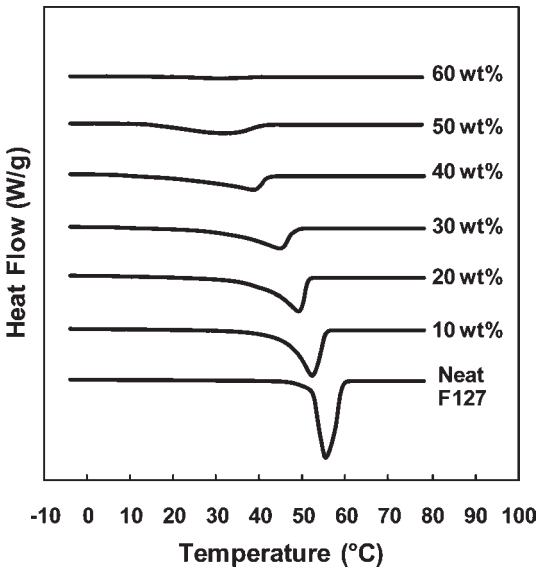

Figure 2. DSC thermograms of F127/IL blends with increasing IL concentration.

qualitatively measured. The heat flow output from the DSC thermograms for all the polymer/IL blends investigated was normalized by the mass of PEO present in the given blend in order to accurately access the crystallinity of the polymer/IL blends.

Figure 2 shows DSC thermograms of F127/IL blends. Thermograms for PEO/IL and copolymer/IL blends with F108 and F77 were also obtained and show similar behavior. For each polymer/IL blend thermogram, the heat flow data were normallized by the mass of PEO present in the given blend. The degree of crystallinity and melting temperature as a function of IL concentration is summarized for each polymer blend in Figure 3. For each series of polymer/IL blends, there is a general decrease in the melting point and PEO crystallinty with increasing IL concentration. At 60 wt % IL concentrations, the crystallinity of F108 and F127 blends is reduced considerably, and with the 60 wt % in F77/IL blend, no melting point was observed.

The crystallinity of the polymer/IL blends was also investigated by wide-angle X-ray scattering (WAXS) and polarized optical microscopy. Figure 4 shows the WAXS profiles of F127/IL blends, obtained at room temperature.

The two main reflections observed for the neat F127 correspond to the (120) and (112) planes of the PEO unit cell. As the concentration of the IL is increased, these peaks become less distinct until only an amorphous halo is observed, in agreement with the calorimetry results. The neat IL has two broad peaks at approximately 9.7 and 14.0 nm^{-1}. The 14.0 nm^{-1} peak corresponds to the interplanar distance between quasi-stracked imidazolium rings, and the 9.7 nm^{-1} peak is assigned to the in-plane cation−cation correlation.[62]

Polarized optical micrographs also demonstrate the effect of IL concentration on crystallinity. Figure 5 shows polarized optical micrographs of F127/IL blends with a range of IL concentrations. As IL concentration is increased, the proportion of material that is not birefringent (amorphous material) appears to increase. With a 60 wt % concentration of IL, only occasional crystallites are still evident. These results are consistent with the calorimetry and WAXS measurements.

Infrared spectroscopy was used to examine interactions between the IL ethylammonium nitrate and Pluronic triblock copolymers. FTIR has been established as a means to

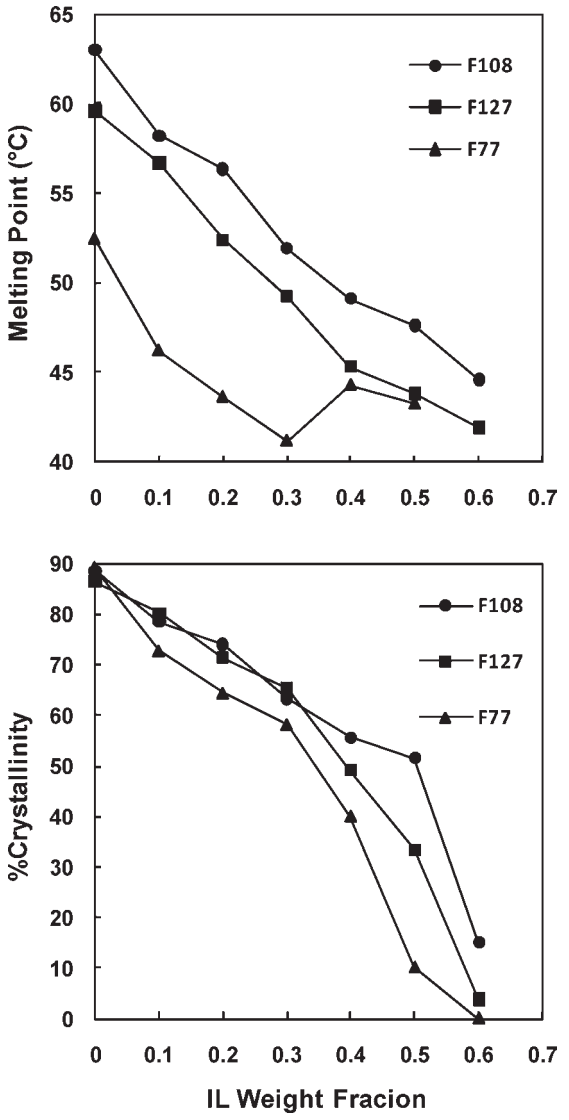

Figure 3. (a) Melting point and (b) percent crystallinity for blends with PEO and with Pluronic copolymers of varying molecular weight and PEO fraction. For each of the thermograms, the heat flow data have been normallized by the mass of PEO present in the blend.

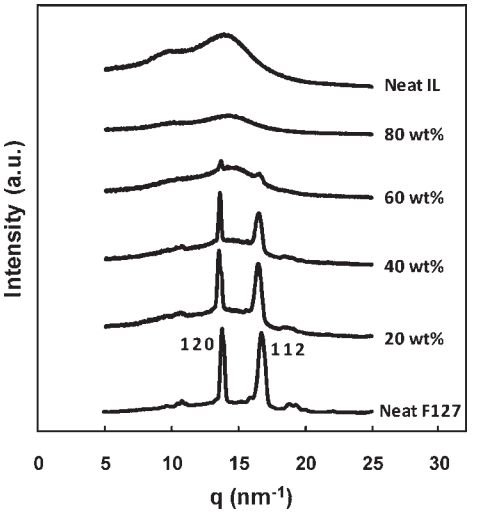

Figure 4. Room temperature WAXS profiles of neat F127, the neat IL, and F127/IL blends with increasing IL concentration.

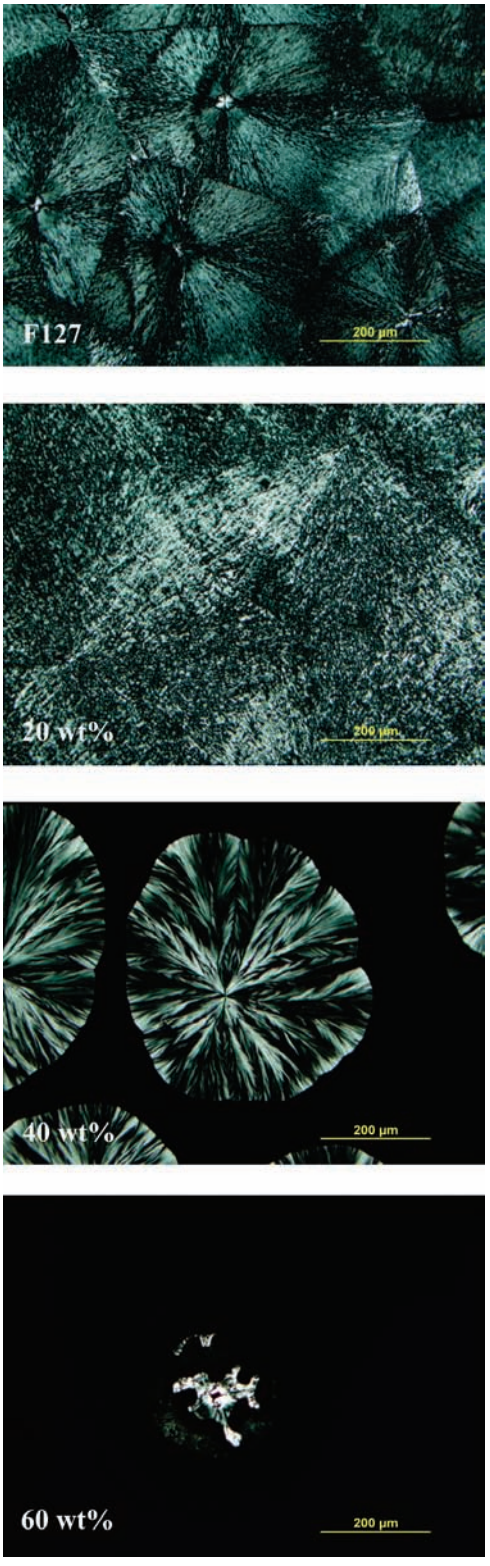

Figure 5. Polarized optical micrographs of F127/IL blends at various IL concentrations.

probe hydrogen bonding in polymers[63,64] and ILs.[65−67] Berg et al.[67] investigated interactions between mixtures of imidazolium-based ILs with chlorine anions and with hexafluorophosphate anions. As the concentration of PF_6^- anions in the mixture was increased, stretching vibrations of CH groups on the imidazolium ring were observed to shift by 40−50 wavenumbers. In the present work, if the ether groups

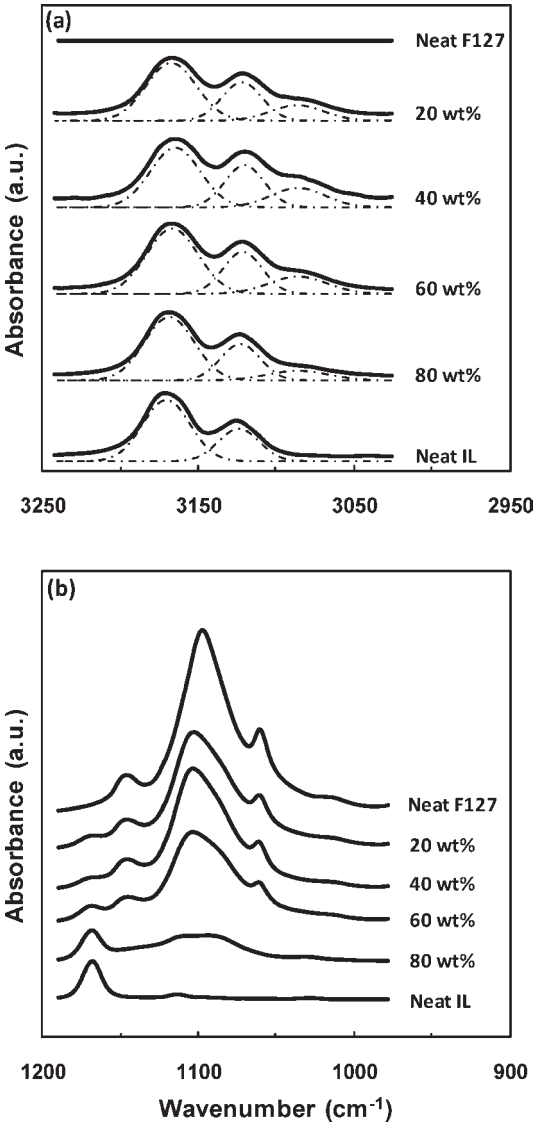

Figure 6. FTIR spectra of F127/IL blends (a) in the imidazolium C−H stretching region of the IL and (b) in the ether stretching region of F127.

on F127 are stronger hydrogen bond acceptors than the PF_6^- anion, the absorbance peaks of the CH stretching vibrations should shift position in comparison to the neat IL. A similar approach has been used to probe hydrogen-bonding interactions between the IL ethylammonium nitrate and PEO microdomains of Pluronic P123[50] and between cellulose triacetate and the IL 1-methyl-3-propylpyrrolidinium bis(trifluoromethylsulfonyl)imide.[39]

Figure 6a shows the infrared spectra for the F127/IL blends in the imidazolium C−H stretching region for the IL. The neat IL has two absorbance peaks in this region at 3170 and 3124 cm^{-1}. These peaks are assigned to asymmetric stretching of the HCCH group and stretching of the CH groups on the imidazolium ring, respectively.[66] The absorbance profile of neat F127 clearly shows that F127 has no absorbance in this wavenumber region. For the F127/IL blends, a shoulder peak is present between 3082 and 3090 cm^{-1}, shifted by ~30 wavenumbers from the CH stretching peak. This shoulder arises from the stretching vibrations of CH groups that have been red-shifted by an interaction with F127. This shift suggests the formation of a hydrogen bond, as H-bonding will dampen the stretching mode vibrations, resulting in the observed red shifts to lower wavenumbers.

The size of the shoulder for the F127/IL blends, and hence the proportion of IL H-bonded to the copolymer, does not vary significantly with IL concentrations in the blend from 20 to 60 wt %. However, at the 80 wt % concentration, the shoulder peak is substantially smaller.

It is possible that at the 80 wt % concentration the IL has saturated all sites capable of H-bonding on the copolymer. Several works have examined hydrogen bonding by imidazolium-based ILs[67−69] and have demonstrated that each of the three ring protons is capable of forming a hydrogen bond. Therefore, it is assumed that each imidazolium ring proton is a hydrogen bond donor, resulting in three donors per IL. It is also assumed that only PEO ether functionalities and no PPO ethers are hydrogen bond acceptors. By these assumptions, at an 80 wt % concentration there are only 0.38 mol acceptors/1 mol donor, suggesting that the hydrogen bond acceptor sites (PEO ethers) are indeed saturated.

Figure 6b shows the FTIR absorbance in the ether stretching region of F127. Neat F127 has three peaks in this region at 1061, 1097, and 1145 cm^{-1}. These peaks correspond to symmetric or asymmetric stretching of the ether group of F127.[70] The neat IL has a strong peak at 1169 cm^{-1} which is assigned to a mixed band of CH_3N and CH_2N stretching and in-plane ring asymmetric stretching.[66] There is also a weak peak at 1113 cm^{-1} assigned to bending of the CH_3N group of the IL.[66] For the F127/IL blends, a shoulder peak on the ether stretching peak at 1097 cm^{-1} is apparent in Figure 6b. The shoulder peak appears to increase in relative intensity as the concentration of IL in the blends is increased. This red-shifted ether shoulder peak indicates that the H-bonding interaction is formed between the IL and the ether groups of the F127.

FTIR spectra of F127/IL blends were compared to PEO/IL and PPO/IL blends at a constant 30 wt % concentration of IL in Figure 7. The spectra in the imidazolium C−H stretching region are shown in Figure 7a and in the ether stretching region in Figure 7b. Both the F127/IL and PEO/IL blends have red-shifted stretching peaks in the imidazolium C−H stretching region and the ether stretching region arising from the interaction of the IL with the ether groups of F127 and PEO.

This interaction does not form in the PPO/IL blend. The blend is optically opaque after agitation, demonstrating that the IL is immiscible with the PPO. This suggests that the methyl group on the PPO chain shields the interaction between the ether oxygen and the IL, and this interaction appears to govern the miscibility of the IL with these polymers. Figure 7 confirms the absence of any interaction between PPO and the IL, as the shoulder peaks present for F127/IL and PEO/IL blends is not observed. The capacity for PEO chains to H-bond to the IL and the lack of this capacity for PPO chains explains the IL selectivity for PEO chains of F127.

It is possible that the peak shifts observed in these spectra are not caused by an H-bonding interaction but rather by an electrostatic interaction. Salt complexation with PEO has been well established by molecular dynamics simulation[71] and experimentally,[5] for which the cation from salts coordinates with the ether oxygen. Shifts in FTIR absorbance peaks have been clearly demonstrated in PEO/Li^+ complexes.[72,73] The imidazolium cation may coordinate with PEO in a similar fashion.

However, other work has demonstrated the ability of ILs to behave as hydrogen bond donors. NMR[69] and infrared spectroscopy[67] have shown that the anion forms hydrogen bonds with protons on the imidazolium ring of the cation. NMR measurements have also shown large downfield proton

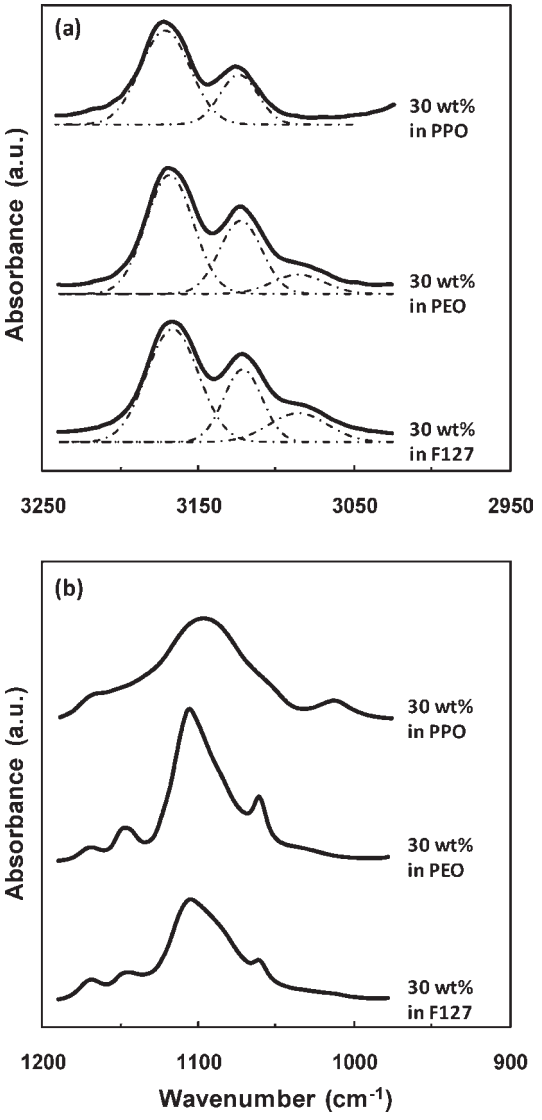

Figure 7. Comparison of FTIR spectra for IL blends in F127 and PEO and PPO homopolymer at constant concentration of IL (a) in the imidazolium C−H stretching region of the IL and (b) in the ether stretching region of F127.

peak shifts when an IL is blended with increasing concentrations of poly(ethyl glycidyl ether), indicating the formation of hydrogen bonds.[68] Solvatochromic probes have shown that ILs have a measurable H-bond acidity by their interaction with the strong hydrogen bond accepting dyes.[74−76] In the present work, regardless of the exact nature of the interaction, it is sufficient to state that infrared spectroscopy demonstrates a favorable enthalpic interaction between the PEO segments of the copolymer and the IL.

Phase Behavior of Blends. Small-angle X-ray scattering has been used to determine the morphologies of the copolymer/IL blends. The scattered intensities are plotted as a function of the scattering vector for blends of the IL in F108, F127, and F77 in Figure 7. The scattering vector is $q = 4\pi/\lambda \sin 2\theta$, where λ is the wavelength of the incident X-ray and θ is the angle between the transmitted and the scattered X-ray intensity. Superscripts above a scattering peak indicate the ratio of the scattering vector at the maximum intensity of the labeled peak to the scattering vector at the maximum of the primary peak.

In Figure 8, a broad peak is observed for the neat copolymers, indicating that the PEO and PPO blocks are

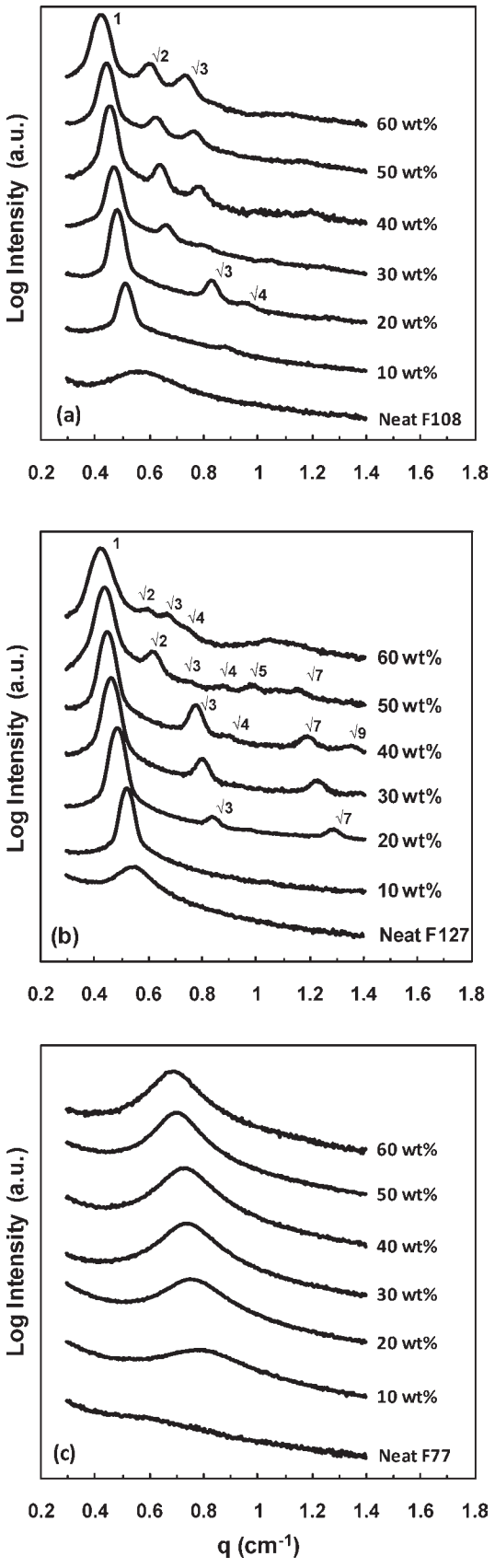

Figure 8. Scattering profiles with increasing IL concentration for blends of IL in (a) F108, (b) F127, and (c) F77.

phase mixed in the melt. There is a large decrease in the width of the peak upon addition of 10 wt % of IL to the F108 and F127 copolymers. With higher concentrations of IL, the peak width is further narrowed and higher order reflections are apparent, indicating an increase in the degree of microphase separation between the two blocks. The IL must therefore be selective for a particular block. It has been demonstrated that the IL is selective for the PEO blocks, as DSC measurements show that the IL forms a favorable enthalpic interaction with the PEO blocks, and the FTIR measurements have confirmed that this interaction does not occur between the IL and PPO.

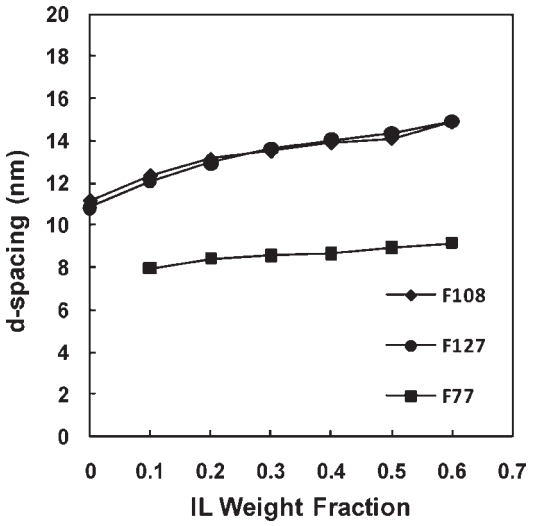

Figure 9. Bragg spacing of the primary scattering peaks for copolymer/IL blends with increasing IL concentration.

The F127 blend with 20 wt % IL has a q_1:$3^{1/2}q_1$:$7^{1/2}q_1$ ratio of peaks for the first- through third-order peaks. This indicates a hexagonal arrangement of cylindrical microdomains, with the minority blocks of PPO forming cylinders in a matrix of PEO swollen with IL. Normally a $2q_1$ peak would be expected, but this peak is often suppressed due to a minimum in the structure factor. The $2q_1$ peak becomes more apparent in the 40 wt % blend, although it is still subdued. Upon increasing the IL concentration to 50 wt %, an order-to-order transition occurs. The peaks show a q_1:$2^{1/2}q_1$:$3^{1/2}q_1$:$4^{1/2}q_1$... pattern. This pattern indicates a change to a body-centered cubic (BCC) arrangement of PPO spheres in a PEO/IL matrix. Increasing the IL concentration to 60 wt % causes the fifth-, sixth-, and seventh-order peaks to combine.

From the SAXS profile, the morphology for F108 blends with 10 wt % of IL is unclear. Considering the volume fraction of the PEO majority block (0.79), the scattering profile most likely represents a cylindrical morphology with only a single higher order peak. The 20 wt % blend is clearly cylindrical, considering the q_1:$3^{1/2}q_1$:$2q_1$ ratio of the higher order peaks. A body-centered cubic morphology is apparent for 30 wt % and greater concentrations of IL. It appears that the Fl08 blends also go through an order-to-order transition.

Increasing the IL concentration in the copolymer blends increases the domain spacing calculated from the primary scattering peak, as shown in Figure 9. The IL selectively swells the PEO microdomains, increasing the distance between PPO microdomains. Selective swelling of the PEO microdomains increases the curvature of the PPO domains, until spherical domains become the stable morphology, and the blends go through the observed order-to-order transitions from cylindrical to spherical morphologies.

Blending IL with F77 does not result in the formation of higher order peaks, although weak microphase separation does occur. Also, blends with F77 do not appear to swell as quickly as the higher molecular weight copolymers. It is

possible that due to the lower molecular weight, the χN product is not large enough to induce strong microphase separation despite the selectivity of the IL additive.

Other work has shown similar behavior, with blends of Pluronic P123 copolymers blended with the ILs [BMI][PF_6][49] and EAN.[50] P123 is also a PEO-*b*-PPO-*b*-PEO copolymer, with 30 wt % PEO blocks. The approximate average molecular weights are 3600 g/mol for the PPO block and 770 g/mol each for the two PEO blocks. SAXS experiments demonstrated that these blends also form ordered morphologies and that order-to-order transitions occur as the IL concentration is altered.[49,50] However, these scattering profiles were attributed to the formation of lyotropic liquid crystals, whereas in the present work, the scattering profiles indicate microphase segregation of a BCP melt. In the previous work with IL blends with P123, the blends display birefringent textures when observed under a polarized optical microscope, indicating the formation of liquid crystalline phases.

The blends of [BMI][PF_6] with the Pluronic copolymers characterized in this work, however, do not appear to form liquid crystals. The birefringent textures of the films displayed in Figure 5 are not characteristic of a liquid crystalline morphology. When these films were heated above the melting temperature, birefringent textures were not observed by polarized optical microscopy. Therefore, the films were completely amorphous in the melt with no liquid crystalline morphology present. Birefringence is expected from lamellar and cylindrical BCP morphologies due to the anisotropy of the copolymer microphases and has been observed by static birefringence measurements.[15,18] In the present work, however, birefringence in the F127/IL melts is not observed by polarized optical microscopy even for blends that microphase separate into a cylindrical morphology. It is possible that the grain size is too small to resolve birefringent textures by optical microscopy.

In addition, the WAXS profiles obtained at room temperature in Figure 4 display peaks corresponding to scattering from (120) and (112) planes, which cannot be characteristic of a liquid crystal and must therefore be from the PEO unit cell. WAXS profiles of F127/IL blends with little or no PEO crystallinity (with 60 and 80 wt % IL concentrations) do not display peaks associated with liquid crystal reflections, only broad peaks associated with IL correlation. Therefore, the SAXS profiles observed in this work are attributed to the microphase separation of the PEO and PPO microdomains.

Conclusions

The phase behavior of blends of the IL 1-butyl-3-methylimidazolium hexafluorophosphate with Pluronic surfactants has been investigated. The IL is selective for the PEO microdomains of the PEO-*b*-PPO-*b*-PEO triblock copolymer Pluronic surfactants. As the concentration of IL in the blends is increased, a large melting point depression of the PEO blocks is observed. This finding indicates a strong, favorable interaction between the IL and PEO. The appearance of a shoulder peak in infrared spectra of F127/IL blends represents the formation of a specific interaction between PEO microdomains and the IL. The formation of a strong, selective interaction between the IL and PEO microdomains enhances the nonfavorable interactions between PEO and PPO microdomains, strengthening microphase segregation in the copolymer melt. This is demonstrated by the SAXS profiles, which show that increasing the IL concentration of the copolymer/IL blends results in the appearance of higher order peaks in the scattering profiles. Increasing the concentration of the IL also causes an order-to-order transition from cylindrical to spherical PPO microdomains. These results demonstrate the potential application of Pluronic copolymers for the generation of ordered ion gels.

References and Notes

(1) Bates, F. S.; Fredrickson, G. H. *Phys. Today* **1999**, *52*, 32–38.
(2) Leibler, L. *Macromolecules* **1980**, *13*, 1602–1617.
(3) Tirumala, V. R.; Romang, A.; Agarwal, S.; Lin, E. K.; Watkins, J. J. *Adv. Mater.* **2008**, *20*, 1603–1608.
(4) Tirumala, V. R.; Daga, V.; Bosse, A. W.; Romang, A.; Ilavsky, J.; Lin, E. K.; Watkins, J. J. *Macromolecules* **2008**, *41*, 7978–7985.
(5) Epps, T. H.; Bailey, T. S.; Pham, H. D.; Bates, F. S. *Chem. Mater.* **2002**, *14*, 1706–1714.
(6) Young, W. S.; Epps, T. H. *Macromolecules* **2009**, *42*, 2672–2678.
(7) Wang, J. Y.; Chen, W.; Roy, C.; Sievert, J. D.; Russell, T. P. *Macromolecules* **2008**, *41*, 963–969.
(8) He, J. B.; Wang, J. Y.; Xu, J.; Tangirala, R.; Shin, D.; Russell, T. P.; Li, X. F.; Wang, J. *Adv. Mater.* **2007**, *19*, 4370–4374.
(9) Ruzette, A. V. G.; Soo, P. P.; Sadoway, D. R.; Mayes, A. M. *J. Electrochem. Soc.* **2001**, *148*, A537–A543.
(10) Lodge, T. P.; Pudil, B.; Hanley, K. J. *Macromolecules* **2002**, *35*, 4707–4717.
(11) Mortensen, K. *J. Phys.: Condens. Matter* **1996**, *8*, A103–A124.
(12) Mortensen, K.; Brown, W.; Jorgensen, E. *Macromolecules* **1994**, *27*, 5654–5666.
(13) Shibayama, M.; Hashimoto, T.; Kawai, H. *Macromolecules* **1983**, *16*, 16–28.
(14) Lai, C. J.; Russel, W. B.; Register, R. A. *Macromolecules* **2002**, *35*, 841–849.
(15) Hanley, K. J.; Lodge, T. P.; Huang, C. I. *Macromolecules* **2000**, *33*, 5918–5931.
(16) Hamley, I. W.; Fairclough, J. P. A.; Ryan, A. J.; Ryu, C. Y.; Lodge, T. P.; Gleeson, A. J.; Pedersen, J. S. *Macromolecules* **1998**, *31*, 1188–1196.
(17) Lodge, T. P.; Xu, X.; Ryu, C. Y.; Hamley, I. W.; Fairclough, J. P. A.; Ryan, A. J.; Pedersen, J. S. *Macromolecules* **1996**, *29*, 5955–5964.
(18) Chandler, C. M.; Vogt, B. D.; Francis, T. J.; Watkins, J. J. *Macromolecules* **2009**, *42*, 4867–4873.
(19) Krossing, I.; Slattery, J. M.; Daguenet, C.; Dyson, P. J.; Oleinikova, A.; Weingartner, H. *J. Am. Chem. Soc.* **2006**, *128*, 13427–13434.
(20) Huddleston, J. G.; Visser, A. E.; Reichert, W. M.; Willauer, H. D.; Broker, G. A.; Rogers, R. D. *Green Chem.* **2001**, *3*, 156–164.
(21) Plechkova, N. V.; Seddon, K. R. *Chem. Soc. Rev.* **2008**, *37*, 123–150.
(22) Weingaertner, H. *Angew. Chem., Int. Ed.* **2008**, *47*, 654–670.
(23) Ueki, T.; Watanabe, M. *Macromolecules* **2008**, *41*, 3739–3749.
(24) Endres, F.; El Abedin, S. Z. *Phys. Chem. Chem. Phys.* **2006**, *8*, 2101–2116.
(25) Sheldon, R. *Chem. Commun.* **2001**, 2399–2407.
(26) Bandres, I.; Montano, D. F.; Gascon, I.; Cea, P.; Lafuente, C. *Electrochim. Acta* **2010**, *55*, 2252–2257.
(27) Noda, A.; Hayamizu, K.; Watanabe, M. *J. Phys. Chem. B* **2001**, *105*, 4603–4610.
(28) Galinski, M.; Lewandowski, A.; Stepniak, I. *Electrochim. Acta* **2006**, *51*, 5567–5580.
(29) Wang, P.; Wenger, B.; Humphry-Baker, R.; Moser, J. E.; Teuscher, J.; Kantlehner, W.; Mezger, J.; Stoyanov, E. V.; Zakeeruddin, S. M.; Gratzel, M. *J. Am. Chem. Soc.* **2005**, *127*, 6850–6856.
(30) Wachter, P.; Zistler, M.; Schreiner, C.; Berginc, M.; Krasovec, U. O.; Gerhard, D.; Wasserscheid, P.; Hinsch, A.; Gores, H. J. *J. Photochem. Photobiol. A: Chem.* **2008**, *197*, 25–33.
(31) Bhattacharya, B.; Lee, J. Y.; Geng, J.; Jung, H. T.; Park, J. K. *Langmuir* **2009**, *25*, 3276–3281.
(32) Kawano, R.; Matsui, H.; Matsuyama, C.; Sato, A.; Susan, M.; Tanabe, N.; Watanabe, M. *J. Photochem. Photobiol. A: Chem.* **2004**, *164*, 87–92.
(33) de Souza, R. F.; Padilha, J. C.; Goncalves, R. S.; Dupont, J. *Electrochem. Commun.* **2003**, *5*, 728–731.
(34) Doyle, M.; Choi, S. K.; Proulx, G. *J. Electrochem. Soc.* **2000**, *147*, 34–37.
(35) Sekhon, S. S.; Park, J. S.; Baek, J. S.; Yim, S. D.; Yang, T. H.; Kim, C. S. *Chem. Mater.* **2010**, *22*, 803–812.
(36) Seki, S.; Kobayashi, Y.; Miyashiro, H.; Ohno, Y.; Mita, Y.; Terada, N.; Charest, P.; Guerfi, A.; Zaghib, K. *J. Phys. Chem. C* **2008**, *112*, 16708–16713.
(37) Seki, S.; Kobayashi, Y.; Miyashiro, H.; Ohno, Y.; Usami, A.; Mita, Y.; Kihira, N.; Watanabe, M.; Terada, N. *J. Phys. Chem. B* **2006**, *110*, 10228–10230.

(38) Ishikawa, M.; Sugimoto, T.; Kikuta, M.; Ishiko, E.; Kono, M. *J. Power Sources* **2006**, *162*, 658–662.
(39) Lee, J. M.; Nguyen, D. Q.; Lee, S. B.; Kim, H.; Ahn, B. S.; Lee, H.; Kim, H. S. *J. Appl. Polym. Sci.* **2010**, *115*, 32–36.
(40) Harner, J. M.; Hoagland, D. A. *J. Phys. Chem. B* **2010**, *114*, 3411–3418.
(41) He, Y. Y.; Boswell, P. G.; Buhlmann, P.; Lodge, T. P. *J. Phys. Chem. B* **2007**, *111*, 4645–4652.
(42) Simone, P. M.; Lodge, T. P. *Macromolecules* **2008**, *41*, 1753–1759.
(43) Virgili, J. M.; Hexemer, A.; Pople, J. A.; Balsara, N. P.; Segalman, R. A. *Macromolecules* **2009**, *42*, 4604–4613.
(44) Simone, P. M.; Lodge, T. P. *ACS Appl. Mater. Interfaces* **2009**, *1*, 2812–2820.
(45) Bai, Z. F.; He, Y. Y.; Lodge, T. P. *Langmuir* **2008**, *24*, 5284–5290.
(46) Meli, L.; Santiago, J. M.; Lodge, T. P. *Macromolecules* **2010**, *43*, 2018–2027.
(47) Ueki, T.; Watanabe, M.; Lodge, T. P. *Macromolecules* **2009**, *42*, 1315–1320.
(48) Lee, J.; Kaake, L. G.; Cho, J. H.; Zhu, X. Y.; Lodge, T. P.; Frisbie, C. D. *J. Phys. Chem. C* **2009**, *113*, 8972–8981.
(49) Wang, L. Y.; Chen, X.; Chai, Y. C.; Hao, J. C.; Sui, Z. M.; Zhuang, W. C.; Sun, Z. W. *Chem. Commun.* **2004**, 2840–2841.
(50) Zhang, G. D.; Chen, X.; Zhao, Y. R.; Ma, F. M.; Jing, B.; Qiu, H. Y. *J. Phys. Chem. B* **2008**, *112*, 6578–6584.
(51) Bai, Z. F.; Lodge, T. P. *Langmuir* **2010**, *26*, 8887–8892.
(52) Atkin, R.; De Fina, L. M.; Kiederling, U.; Warr, G. G. *J. Phys. Chem. B* **2009**, *113*, 12201–12213.
(53) Zheng, L.; Guo, C.; Wang, J.; Liang, X. F.; Chen, S.; Ma, J. H.; Yang, B.; Jiang, Y. Y.; Liu, H. Z. *J. Phys. Chem. B* **2007**, *111*, 1327–1333.
(54) Zhang, S. H.; Li, N.; Zheng, L. Q.; Li, X. W.; Gao, Y. A.; Yu, L. *J. Phys. Chem. B* **2008**, *112*, 10228–10233.
(55) Anderson, J. L.; Pino, V.; Hagberg, E. C.; Sheares, V. V.; Armstrong, D. W. *Chem. Commun.* **2003**, 2444–2445.
(56) Wang, Z. N.; Liu, F.; Gao, Y.; Zhuang, W. C.; Xu, L. M.; Han, B. X.; Li, G. Z.; Zhang, G. Y. *Langmuir* **2005**, *21*, 4931–4937.
(57) Zhuang, W. C.; Chen, X.; Cai, J. G.; Zhang, G. D.; Qiu, H. Y. *Colloids Surf., A* **2008**, *318*, 175–183.
(58) Sakai, H.; Saitoh, T.; Endo, T.; Tsuchiya, K.; Sakai, K.; Abe, M. *Langmuir* **2009**, *25*, 2601–2603.
(59) Araos, M. U.; Warr, G. G. *J. Phys. Chem. B* **2005**, *109*, 14275–14277.
(60) Atkin, R.; Bobillier, S. M. C.; Warr, G. G. *J. Phys. Chem. B* **2010**, *114*, 1350–1360.
(61) Hong, S.; Yang, L. Z.; MacKnight, W. J.; Gido, S. P. *Macromolecules* **2001**, *34*, 7009–7016.
(62) Triolo, A.; Mandanici, A.; Russina, O.; Rodriguez-Mora, V.; Cutroni, M.; Hardacre, C.; Nieuwenhuyzen, M.; Bleif, H. J.; Keller, L.; Ramos, M. A. *J. Phys. Chem. B* **2006**, *110*, 21357–21364.
(63) Skrovanek, D. J.; Howe, S. E.; Painter, P. C.; Coleman, M. M. *Macromolecules* **1985**, *18*, 1676–1683.
(64) Coleman, M. M.; Skrovanek, D. J.; Hu, J. B.; Painter, P. C. *Macromolecules* **1988**, *21*, 59–65.
(65) Cammarata, L.; Kazarian, S. G.; Salter, P. A.; Welton, T. *Phys. Chem. Chem. Phys.* **2001**, *3*, 5192–5200.
(66) Talaty, E. R.; Raja, S.; Storhaug, V. J.; Dolle, A.; Carper, W. R. *J. Phys. Chem. B* **2004**, *108*, 13177–13184.
(67) Berg, R. W.; Deetlefs, M.; Seddon, K. R.; Shim, I.; Thompson, J. M. *J. Phys. Chem. B* **2005**, *109*, 19018–19025.
(68) Tsuda, R.; Kodama, K.; Ueki, T.; Kokubo, H.; Imabayashi, S.; Watanabe, M. *Chem. Commun.* **2008**, 4939–4941.
(69) Avent, A. G.; Chaloner, P. A.; Day, M. P.; Seddon, K. R.; Welton, T. *J. Chem. Soc., Dalton Trans.* **1994**, 3405–3413.
(70) Dissanayake, M.; Frech, R. *Macromolecules* **1995**, *28*, 5312–5319.
(71) Siqueira, L. J. A.; Ribeiro, M. C. C. *J. Chem. Phys.* **2005**, 122.
(72) Frech, R.; Chintapalli, S.; Bruce, P. G.; Vincent, C. A. *Macromolecules* **1999**, *32*, 808–813.
(73) Lin, J. H.; Woo, E. M.; Huang, Y. P. *J. Polym. Sci., Part B: Polym. Phys.* **2006**, *44*, 3357–3368.
(74) Crowhurst, L.; Mawdsley, P. R.; Perez-Arlandis, J. M.; Salter, P. A.; Welton, T. *Phys. Chem. Chem. Phys.* **2003**, *5*, 2790–2794.
(75) Lungwitz, R.; Friedrich, M.; Linert, W.; Spange, S. *New J. Chem.* **2008**, *32*, 1493–1499.
(76) Reichardt, C. *Green Chem.* **2005**, *7*, 339–351.